# A Comparison between Artificial Neural Network Prediction Models for Coronal Hole Related High-Speed Streams

Rehab Abdulmajed, Amr Hamada, Ahmed Elsaid, Hisashi Hayakawa, Ayman Mahrous

*Abstract*—Solar emissions have a high impact on the Earth's magnetic field, and the prediction of solar events is of high interest. Various techniques have been used in the prediction of the solar wind using mathematical models, MHD models and neural network (NN) models. This study investigates the coronal hole (CH) derived high-speed streams (HSSs) and their correlation to the CH area and create a neural network model to predict the HSSs. Two different algorithms were used to compare different models to find a model that best simulated the HSSs. A dataset of CH synoptic maps through Carrington rotations 1601 to 2185 along with Omni-data set solar wind speed averaged over the Carrington rotations is used, which covers Solar Cycles (SC) 21, 22, 23, and most of 24.

*Keywords*—Artificial Neural Network, ANN, Coronal Hole Area Feed-Forward neural network models, solar High-Speed Streams, HSSs.

## I. INTRODUCTION

THE study of space weather has a crucial role in modern technology development, as these technologies require a full understanding of space weather, and its effects on satellites and Earth as well. Geomagnetic disturbances have destructive effects on modern space technology and Earth's communication system [1]. Solar wind speed (SW) is a continuous plasma flow into the interplanetary magnetic field, the interaction of this high-speed flow causes disturbance in the Earth's magnetic field [2]. The High-Speed Solar Wind Streams (HSSs) are emitted from the Coronal Holes (CHs) [3], which are dark areas with reduced temperature than their surroundings on the solar corona [4]. The interaction between the slow SW speed and the coronal hole-related HSSs results in a shock region occurring due to the co-rotation of the sun (CIR) [5].

Various research groups used different methods to study the relationship between the HSSs and coronal hole area (A). Statistical studies are performed on single low latitude CHs and their correlation to the peak velocity of the coronal hole-derived HSSs [6]–[8], while [9] averaged the total area of coronal holes covering the solar disk from 1967 to 1988 over 3 months, they resulted in a correlation with the 3-month average

of the measured HSSs. These studies showed a correlation between the area traversed by the central meridian CH and the HSSs. The magnitude of the correlation coefficient (cc) depends on the solar cycle of the studied period. Besides, the location of the coronal hole, the highest cc was detected in the declining and uprising phases of the solar cycle [10], [11].

Furthermore, [10] extended their study to a period of a low CME activity, the declining phase of cycle 23 to obtain cross-correlation functions to forecast the solar wind parameters. In addition, they deduced that the meridional-located CH correlates fairly with the HSSs peak velocity, while [9] and [12] deduced that depending on the location of the coronal hole, the correlation decreases with the elimination of polar CHs. Also, they correlated the meridional CHs with the Dst index generated from the impact of the fast solar wind streams. To study this relationship within a wide range of data, [3] spread out to analyze the variations of CH-related HSSs for the solar cycles 23 and 24, which showed a constructive correlation between the maximum values of both CH and solar wind speed with larger values of cc for the solar cycle 23 than 24 as a result of the larger area for CH and faster SW flow in the cycle 23.

An Artificial Neural Network (ANN) is a simulation of the human brain with its complexity and ability to process information and transmit it to the neurons and receptors [13]. Throughout an activation function, it transmits data from an input layer to artificial nodes (neurons) connected to a weighted sum [14]. Recently, various ANN models with different algorithms were developed to solve non-linear systems problems [15]. ANN techniques are widely used in the study of space weather due to their ability to analyze large data sets and compute non-linear relationships with high accuracy [1]. Different ANN techniques were used by various research groups to predict solar activity, geomagnetic activity, communication activity, and the satellite drag effect [1], [16].

The Feed forward back propagation (FFBP) network is a simple basic form of ANN [15]. Two models of FFBP are implemented using the Levenberg-Marquardt (LM) and Bayesian-Regularization (BR) algorithms to obtain the best-performing network for our data set.

The network is based on predicting the solar HSSs over a Carrington Rotation (CR) average for the period CR:1601 to CR:2185 using the CH area data set as an input parameter. The CH area dataset is obtained from Oulu University Archive, SW data with a one-day resolution are available on the Omni-Web dataset.

R.Abdulmajed is with the Space Environment department, Egypt-Japan University of Science and Technology (E-JUST), Alexandria, Egypt (e-mail: Rehab.abdo@ejust.edu.eg).

A.Hamada is with the Space Physics and Astronomy Research Unit, University of Oulu, Finland and Physics Department, Faculty of Science, Helwan University, Cairo, Egypt.

A.Mahrous and A.Elsaid are with Egypt-Japan University of Science and Technology (E-JUST), Alexandria.

H.Hayakawa is with Nagoya University, Nagoya University, Japan.

World Academy of Science, Engineering and Technology
International Journal of Physical and Mathematical Sciences
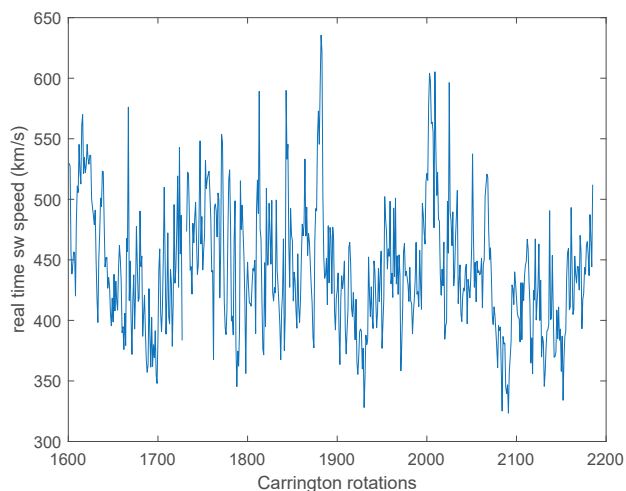Vol:18, No:5, 2024

Fig. 1 SW speed averaged over the Carrington rotation from CR:1601 to CR:2185 on the y-axis; the CR on the x-axis
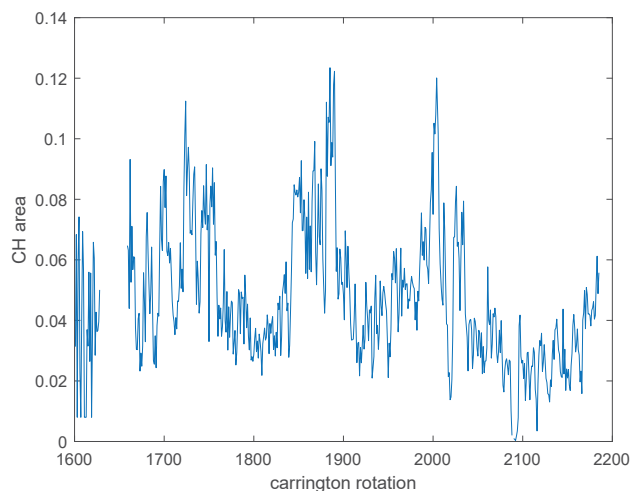


Fig. 2 CH area on the y-axis with the Carrington rotations on the x-axis

Detailed information about the dataset and the network implementation is represented in Section II, and Results and Discussion in Section III.

## II. METHODOLOGY

A simple feed-forward with back-propagation technique is used to create a prediction model for the HSSs. A comparison between the Bayesian Regularization (BR) and the Levenberg-Marquardt (LM) algorithms to show the difference between them in terms of the Root Mean Square Error (RMSE) and correlation between target and output (R-value), the model implementation and the choice of hyperparameters are detailed in Section II-B. Data analysis performed on the CH and SW datasets are explained in Section II-A.

### A. Data Acquisition and Analysis

An interval of 44 years (1973-2017) that covers SCs 21,22,23 and most of SC 24 is used in this study. Solar wind data are obtained from the NASA/NSSDC OMNI dataset [17]. The SW dataset was averaged over a Carrington rotation average, and then we added two filtration steps. First, we used the Richardson and Cane catalog for CME, and CIR [18] which classifies the solar wind into four categories using a numbering code, where: (1) CME/Interplanetary-CME related flow. (2) HSSs, with SW speed V > 450 Km/s. (3) Slow solar wind. (4) Unclear event. We used this categorization to exclude CME-driven, unclear events, and the slow SW; thus the analysis focuses only on the CIR-associated HSSs. Afterward, due to the lack of data between the years 1983 and 1994, another filtration is applied to the dataset to exclude the CR of more than 25% missing data. A representation of the SW on a CR averaged is illustrated in Fig. 1.

Within the same interval, the CH area dataset for each CR has a total of 586 Carrington rotations starting from CR:1601 to CR:2185. CH area is obtained from a developed list [19] using the SOHO/EIT and SDO/AIA homogeneous synoptic
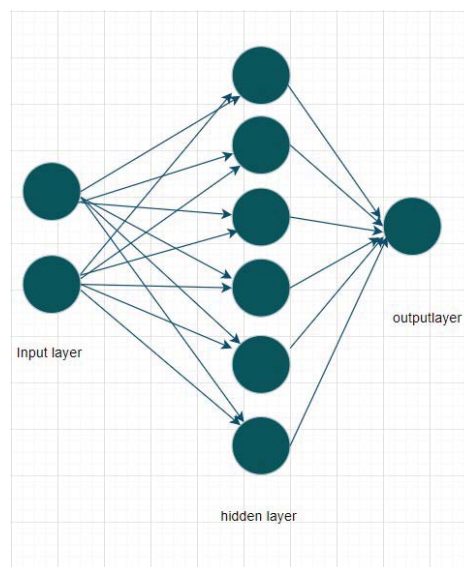


Fig. 3 Single layer FFBP Network architecture consisting of an input layer, hidden layer of 6 neurons, and an output layer

maps and the McIntosh archive (McA) [20]. These data are represented in Fig. 2.

### B. Neural Network

A supervised learning algorithm is used in our ANN; the back-propagation technique is mostly used; it automatically updates the weights with gradient vector [14]. A single-layer FFBP network is used, which consists of an input layer, one hidden layer, and an output layer, as represented in Fig. 3. The inputs are divided into training, validating, and testing sets. The hidden number of nodes is defined by a comparison between the root mean squared error of the training set (RMSE train) and the testing set (RMSE test). The difference between the RMSE-test and RMSE-train is referred to as the $\Delta$-RMSE. The criterion for choosing the number of nodes is basically testing the network over several numbers of neurons (n) and

World Academy of Science, Engineering and Technology
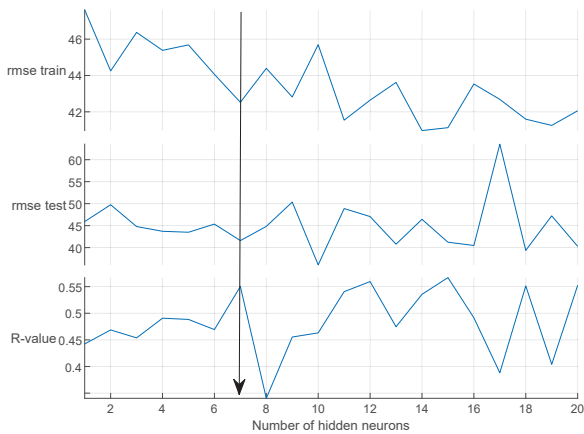International Journal of Physical and Mathematical Sciences
Vol:18, No:5, 2024

Fig. 4 Comparison between the RMSE-train, RMSE-test, and the R-value (from the top on the y-axis) with the number of neurons on the x-axis for the LM-algorithm; the black vertical arrow points out to the best number of neurons
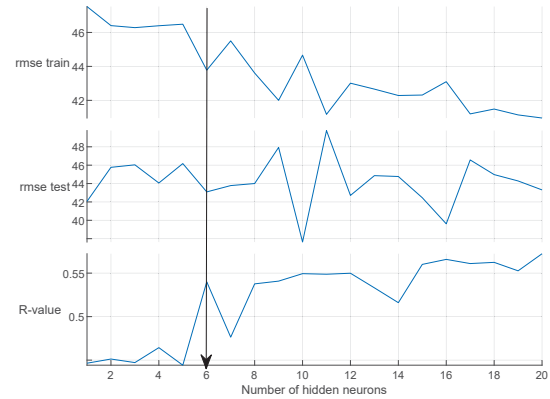


Fig. 5 Comparison between the RMSE-train, RMSE-test, and the R-value (from the top on the y-axis) with the number of neurons on the x-axis for the BR- algorithm; the black vertical arrow points out to the best number of neurons

TABLE I
RMSE RESULTS OF (LM) AND (BR) ALGORITHMS

| algorithm | RMSE-train (km/s) | RMSE-test (km/s) | Δ-RMSE | n |
|---|---|---|---|---|
| LM-algorithm | 41.9341 | 50.5205 | 8.5864 | 7 |
| BR-algorithm | 45.2372 | 47.6045 | 2.3673 | 6 |

TABLE II
CORRELATION RESULTS OF (LM) AND (BR) ALGORITHMS

| algorithm | R-train | R-test | R-value | n |
|---|---|---|---|---|
| LM-algorithm | 0.57473 | 0.3383 | 0.5155 | 7 |
| BR-algorithm | 0.48765 | 0.4056 | 0.4697 | 6 |

choosing the lowest value of Root Mean Square Error (RMSE) that corresponds to the highest correlation factor (R-value).

For the LM algorithm, the dataset is divided into a 70% training set, a 15% validating set, and a 15% testing set. The network is tested over (1-20) neurons to validate the model's best number of neurons. Fig. 4 illustrates the RMSE-train, RMSE-test, and the R-value over a number of hidden neurons (n). The best n represents the highest R-value with the lowest RMSE-train and RMSE-test (vertical arrow). This model's optimum number of neurons is n = 7, as it presents the least RMSE value with the highest R-value. Lower values of RMSE can be seen in this figure, but it is advisable to choose the first minimum of RMSE that corresponds to a peak in the R-value to avoid the over-fitting of the model [21].

For the BR-algorithm, the same criterion was applied but for the dataset division, it is divided into a training set of 75% and a testing set of 25%. This is because the Br-algorithm can perform the validation process on datasets with a low chance of over-fitting due to its statistical process [22]. An illustration of the RMSE-train, RMSE-test, and the R-value over a number of hidden neurons (n) for the BR-algorithm is represented in Fig. 5 showing the best (n) for this model (vertical arrow).

## III. RESULTS AND DISCUSSION

After the implementation of each model, we present each model by plotting the regression between the real and predicted SW for the training, testing, and validating (if exist) sets, this is represented in Fig. 6 for the LM-model, and Fig. 7 for the BR-model.

The comparison between the models depends on two aspects, the RMSE, and the R-value. The phase of the result, whether it is training or testing, indicates that the better the testing results, the better the model is [23]. The training set is essential for the learning process. Its results show how far the model can learn the relationship between the inputs and outputs, while the testing set shows how the model will be able to predict new data after the learning process.

An illustration of the RMSE results (training and testing) for the (LM) and (BR) models is represented in Table I, and the resulting correlation for each set is presented in Table II.

These results show a lower RMSE-test for the BR- model than the LM- model, while for the RMSE-train, a lower RMSE value is for the LM-model. While, for the correlation scale, the BR- model shows a better correlation than the lm-model in the testing phase. On the other hand, the LM-model has a higher correlation in the training phase and the overall correlation.

Fig. 6 shows the linear regression results for the training, validation, and testing sets, and the overall regression between the target (real SW speed), and the output (predicted SW speed) and shows the correction equation on the y-axis of each graph. By the same token, Fig. 7 represents the linear regression for the training, and testing sets and the overall regression between the target and the output result.

## IV. CONCLUSION

Although the overall correlation is higher in the LM-model and the training RMSE and R-value results are better, but also Δ-RMSE is of a higher value. Thus, the difference between training and testing RMSE results is higher. However, in the case of the BR-model, the testing RMSE and R-value results are better than the LM-model, and the Δ-RMSE is much lower than that of the LM-model. The variable Δ-RMSE is an indicator of the consistency of the network, the closer gap

World Academy of Science, Engineering and Technology
International Journal of Physical and Mathematical Sciences
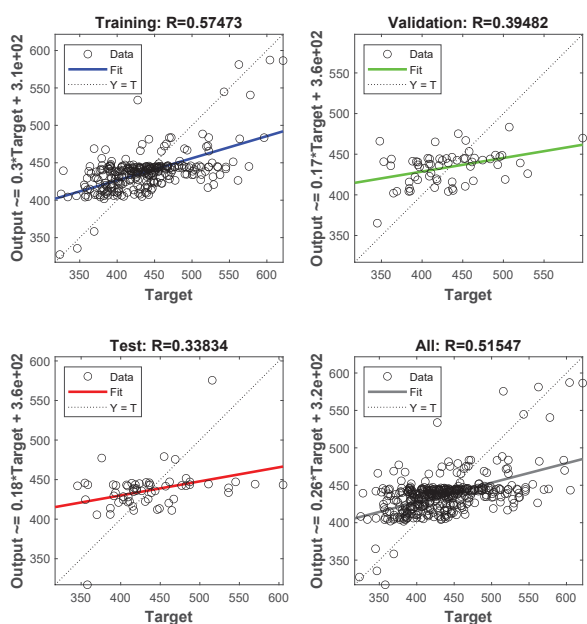Vol:18, No:5, 2024

Fig. 6 Training, validation, testing, and overall regression between the real and resulted data for the LM-algorithm
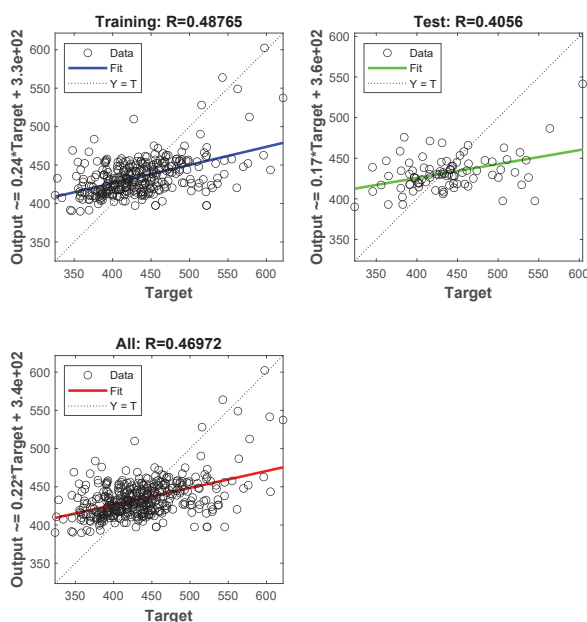


Fig. 7 Training, testing, and overall regression between the real and resulted data for the BR-algorithm

between the RMSE-train and RMSE-test shows more reliable output results of the network, even with a slightly higher overall correlation. When it comes to the prediction, the model should have better testing results as they are speaking of the ability of the model to blindly predict the desired output. Thus, we can conclude that the BR-model is considered a better-performing prediction model as it has better results in the testing phase, which means that it can predict the target more accurately than the LM-model. The BR- model can

predict the SW speed using the CH area with a correlation coefficient of 0.46972 and an RMSE of 45.5326 km/s.

Moreover, the LM-model has better results in terms of the correlation between the input real SW speed and the predicted output. It can predict the SW speed through the CH area as an input to the network with a correlation of R= 0.5155 and an error of RMSE= 44.2169 km/s.

Overall, there is a slight difference in the values of the R-value and the RMSE between both models. Although the BR-model has a better prediction performance than the LM-model, the LM-model has a higher correlation than the BR- model. These findings are confined to the used dataset, and the choice of the model depends on the type and length of the data.

## ACKNOWLEDGMENT

## REFERENCES

[1] Y. Yang, F. Shen, Z. Yang, and X. Feng, "Prediction of solar wind speed at 1 au using an artificial neural network," *Space Weather*, vol. 16, no. 9, pp. 1227–1244, 2018.
[2] V. Upendran, M. C. Cheung, S. Hanasoge, and G. Krishnamurthi, "Solar wind prediction using deep learning," *Space Weather*, vol. 18, no. 9, p. e2020SW002478, 2020.
[3] Y. Nakagawa, S. Nozawa, and A. Shinbori, "Relationship between the low-latitude coronal hole area, solar wind velocity, and geomagnetic activity during solar cycles 23 and 24," *Earth, Planets and Space*, vol. 71, no. 1, pp. 1–15, 2019.
[4] S. R. Cranmer, "Coronal holes," *Living Reviews in Solar Physics*, vol. 6, pp. 1–66, 2009.
[5] S. J. Hofmeister, A. Veronig, M. Temmer, S. Vennerstrom, B. Heber, and B. Vršnak, "The dependence of the peak velocity of high-speed solar wind streams as measured in the ecliptic by ace and the stereo satellites on the area and co-latitude of their solar source coronal holes," *Journal of Geophysical Research: Space Physics*, vol. 123, no. 3, pp. 1738–1753, 2018.
[6] J. Nolte, A. Krieger, A. Timothy, R. Gold, E. Roelof, G. Vaiana, A. Lazarus, J. Sullivan, and P. McIntosh, "Coronal holes as sources of solar wind," *Solar Physics*, vol. 46, no. 2, pp. 303–322, 1976.
[7] V. Abramenko, V. Yurchyshyn, and H. Watanabe, "Parameters of the magnetic flux inside coronal holes," *Solar Physics*, vol. 260, no. 1, pp. 43–57, 2009.
[8] N. V. Karachik and A. A. Pevtsov, "Solar wind and coronal bright points inside coronal holes," *The Astrophysical Journal*, vol. 735, no. 1, p. 47, 2011.
[9] Y.-M. Wang and N. Sheeley Jr, "Magnetic flux transport and the sunspot-cycle evolution of coronal holes and their wind streams," *The Astrophysical Journal*, vol. 365, pp. 372–386, 1990.
[10] B. Vršnak, M. Temmer, and A. M. Veronig, "Coronal holes and solar wind high-speed streams: I. forecasting the solar wind parameters," *Solar Physics*, vol. 240, no. 2, pp. 315–330, 2007.
[11] S. Robbins, C. Henney, and J. Harvey, "Solar wind forecasting with coronal holes," *Solar Physics*, vol. 233, pp. 265–276, 2006.
[12] B. Vršnak, M. Temmer, and A. M. Veronig, "Coronal holes and solar wind high-speed streams: Ii. forecasting the geomagnetic effects," *Solar Physics*, vol. 240, pp. 331–346, 2007.
[13] H. Simon, *Neural networks: a comprehensive foundation*. Prentice hall, 1999.
[14] M. H. Sazli, "A brief review of feed-forward neural networks," *Communications Faculty of Sciences University of Ankara Series A2-A3 Physical Sciences and Engineering*, vol. 50, no. 01, 2006.

[15] J. Lazzús, P. Vega, P. Rojas, and I. Salfate, "Forecasting the dst index using a swarm-optimized neural network," *Space Weather*, vol. 15, no. 8, pp. 1068–1089, 2017.

[16] H. Lundstedt, "Progress in space weather predictions and applications," *Advances in Space Research*, vol. 36, no. 12, pp. 2516–2523, 2005.

[17] "Nasa/nssdc omni dataset." [Online]. Available: https://omniweb.gsfc.nasa.gov/

[18] I. G. Richardson and H. V. Cane, "Solar wind drivers of geomagnetic storms during more than four solar cycles," *Journal of Space Weather and Space Climate*, vol. 2, p. A01, may 2012. [Online]. Available: http://www.swsc-journal.org/10.1051/swsc/2012001

[19] A. Hamada, T. Asikainen, and K. Mursula, "A uniform series of low-latitude coronal holes in 1973–2018," *Solar Physics*, vol. 296, no. 2, pp. 1–22, 2021.

[20] "Noaa national centers for environmental information," mcIntosh archive Dataset. [Online]. Available: https://www.ngdc.noaa.gov/stp/space-weather/solar-data/solar-imagery/composites/synoptic-maps/mc-intosh/

[21] K. Yotov, E. Hadzhikolev, and S. Hadzhikoleva, "Determining the number of neurons in artificial neural networks for approximation, trained with algorithms using the jacobi matrix," *TEM Journal*, vol. 9, no. 4, p. 1320, 2020.

[22] F. Burden and D. Winkler, "Bayesian regularization of neural networks," *Artificial neural networks: methods and applications*, pp. 23–42, 2009.

[23] J. M. Caswell, "A nonlinear autoregressive approach to statistical prediction of disturbance storm time geomagnetic fluctuations using solar data," *Journal of Signal and Information Processing*, vol. 2014, 2014.

[24] "University of oulu database of solar euv and coronal hole synoptic maps." [Online]. Available: http://satdat.oulu.fi/solar_data